Brain tissue segmentation of fetal MR images

M. Bach Cuadra[1], M. Schaer[1,2], A. André[1],
L. Guibaud[3], S. Eliez[2], and J.-Ph. Thiran[1]

[1] Signal Processing Laboratory (LTS5), Ecole Polytechnique Fédérale de Lausanne, Switzerland, Meritxell.Bach@epfl.ch,JP.Thiran@epfl.ch,
[2] Service Médico-Pédagogique, Psychiatry Department, University of Geneva School of Medicine, Switzerland, Marie.Schaer@unige.ch
[3] Imagerie pédiatrique et fœtale, Hôpital Debrousse, Lyon, France. ⋆

Abstract. We present a segmentation method for fetal brain tissues of T2w MR images, based on the well known Expectation Maximization Markov Random Field (EM-MRF) scheme. Our main contribution is an intensity model composed of 7 Gaussian distribution designed to deal with the large intensity variability of fetal brain tissues. The second main contribution is a 3-steps MRF model that introduces both local spatial and anatomical priors given by a cortical distance map. Preliminary results on 4 subjects are presented and evaluated in comparison to manual segmentations showing that our methodology can successfully be applied to such data, dealing with large intensity variability within brain tissues and partial volume (PV).

1 Introduction

Development of the fetal brain surface, which characterizes gyration, is one of the major maturational processes of the human brain. Fetal MRI [1, 2] is now a well recognized tool for cerebral anatomy evaluation, especially for analysis of the cortex. However, this analysis remains qualitative using the progressive identification of the primary and secondary gyri along the second and third trimesters of the pregnancy. A quantitative analysis of fetal cortical surface can represent a new approach which can be used as a marker of the cerebral maturation and also for studying central nervous system pathologies. However, this quantitative approach is a major challenge for several reasons. First, movement of the fetus inside the amniotic cavity requires very fast MRI sequences to minimize motion artifacts, resulting in a poor spatial resolution and/or lower SNR. Second, due to the ongoing myelination and cortical maturation, the appearance of the developing brain differs very much from the homogenous tissue types found in adults. Third, due to low resolution, fetal MR images considerably suffer of partial volume (PV) effect, sometimes in large areas. Early brain development has been studied quantitatively with the use of cerebral MRI obtained from premature

⋆ This work was supported by the Center for Biomedical Imaging (CIBM) of the Geneva–Lausanne Universities and the EPFL, as well as the foundations Leenaards and Louis-Jeantet.

neonates [3–6]. However, this strategy does not allow the study of normal brain development over a large age range, since the most premature births are not likely to represent appropriate specimen for the study of normal development.

This paper presents a segmentation method for fetal brain tissues of T2w MR images. To our knowledge, there is only two studies concerning the automated segmentation of MR fetal imaging: in [7] some specific areas of the fetal brain (posterior fossa, brainstem and vermis) were segmented on a single slice by region growing algorithm and, recently in [8] the germinal matrix was segmented using atlas-based techniques.

1.1 Related work on neonate segmentation

Pioneer studies on newborn and preterm infants were carried out using k-nearest neighbor (KNN) algorithm [9] using different sequences (T1w, PD and T2w). This approach has been applied to several studies for brain development in both premature and mature newborns [4, 10, 11]. Recently, a similar approach using T2w and inversion recovery (IR) sequences has been suggested [12]. Atlas-based segmentation is also applied to newborn [6] using T1w and T2w sequences. In their framework, as for KNN approaches, the use of probabilistic atlases is crucial to overcome the intensity contrast limitations. Bayesian frameworks have been also suggested for neonatal brain segmentation [3, 5, 13]. Among them, the Expectation Maximization Markov Random Field (EM-MRF) scheme has been applied to segment cortical GM (CoGM), unmyelinizated WM, and CSF in [3]. The MRF scheme allows them to tackle the PV misclassified voxels between CSF and GM.

Newborns usually fall asleep during the acquisition process, and a suction-evacuated pillow can be used to immobilize them, while shorter acquisitions have to be used in fetal MRI to avoid motion. Thus, compared to newborn images, fetal MRI has lower resolution and higher PV. In our opinion, PV must then be explicitly considered in the segmentation algorithm. Most of existing segmentation methods in newborns use multispectral data (T1w and T2w but also PD and IR) allowing a more accurate distinction between different tissue types. However, such data is rarely available for fetal MRI where T2w is often the only one. Consequently, performance of such approaches when using one modality only may decrease. Finally, statistical priors coming from a template or probabilistic atlases are often needed in conjunction with the above methods. Such input is not available at this point for fetus, thus most of these atlas-based methods cannot be applied. Moreover, construction of fetal atlases is very challenging due to the huge variability of anatomy in first weeks of gestation and the low contrast-to-noise ratio. However, with a reliable automatic segmentation of brain tissues in fetal MRI such priors could be constructed afterwards.

Our approach is inspired from the EM-MRF scheme in [3] and from our previous work in [14]. Our main contribution is an intensity model composed of 7 Gaussian distribution. After an initial Bayesian segmentation, the final segmentation is done by Maximum a Posteriori (MAP) on a MRF scheme. The

second main contribution is a 3 step MRF model that will introduce both local spatial priors and anatomical priors given by a cortical distance map.

2 Material and Methodology

Prenatal MR imaging was performed with a 1-T system (GE Medical Systems, Milwaukee) using single shot fast spin echo sequences (TR 7000 ms, TE 180 ms, FOV 40 x 40 cm, slice thickness $5.4mm$, in plane spatial resolution $1.09mm$). Each fetus has 6 axial volumes (around 15 slices per volume), each of them acquired in about 1 min. Each volume is *shifted* by 1 mm with respect to the previous one. Gestational age (GA) ranged from 29 to 32 weeks.

The first step of the segmentation process is to segment the brain volume since our tissue model does not take non-brain tissues into account. Currently, this is done manually since our data contain in fact very few slices but atlas-based segmentation could be used for larger data set. The second pre-processing step is the bias field correction [15,16][4]. After that, an intensity linear normalization is performed to have intensity values that range from 0 to 255. Note that due to intra-tissue variability of developing brain some intensity variability still remain.

2.1 Image model

A Finite Gaussian Mixture Model (FGMM) is used to fit the image intensity. While modeling the observed intensity by Gaussian probability density functions (PDFs) can be justified in adult brain MRI, this can be more questionable in fetal MRI [6,13]. For this reason, and to cope with the large variability of intensity in GM and WM, we propose a 7 PDFs model, $L = \{GM_1, GM_2, C_1, WM_1, WM_2, C_2, CSF\}$. We propose to use a mixture of 2 Gaussians (GM_1 and GM_2, WM_1 and WM_2) to model the pure tissues. The use of two *transition* classes, C_1 and C_2, re-enforces also the non-Gaussian modeling of CSF, GM and WM tissues. The advantage of using these *transition* classes is twofold. First, they improve the robustness of the observed data (the image intensity) estimation. Second, they allow to explicitly take them into account in the MRF scheme and re-classify them according to spatial information. The optimization problem is solved through the EM algorithm and the setting of initial parameters is automatized for all GAs: $\mu_{GM_1} = 30$, μ_{WM_1} is the gray level of the highest pick of the histogram, Max(h) in Fig. 1, and $\mu_{CSF} = 90$; the rest of initial means are evaluated accordingly to the rule in Fig. 1, that is as proportions of $A, \mu_{WM_1} - \mu_{GM_1}$, and $B, \mu_{CSF} - \mu_{WM_1}$, values; standard deviations are initialized as [0.20.20.20.10.10.30.3]; initial weights are set to $\frac{1}{7}$. These values have been found empirically on the current data set. The distribution of classes according to PDFs is represented in Table 1. The labels $L = \{GM, C_1, WM, C_2, CSF\}$ render the large variety of tissues. For instance,

[4] This step is necessary because our tissue classification algorithm does not model the bias nor iterates between bias estimation and tissue classification as other methods do such as in [17] for instance.

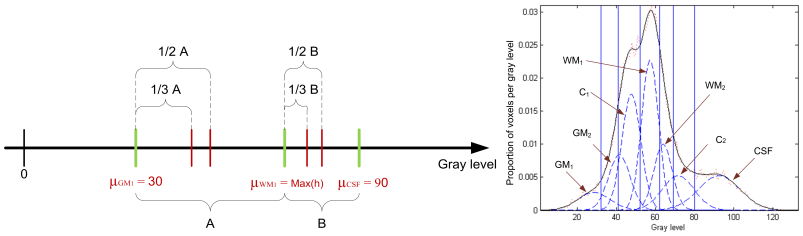

Fig. 1. Initial mean values μ_{GM_1}, μ_{WM_1}, and μ_{CSF} are set first. Max(h) is the gray level of the highest pick of the histogram. The rest of mean values are defined as proportions of $A = \mu_{WM_1} - \mu_{GM_1}$, and $B = \mu_{CSF} - \mu_{WM_1}$ values. Fitted PDFs: intensity histogram (red), fitted histogram (black), and PDFs (blue).

gray matter is represented by labels GM and C_1. GM mainly represents cortical GM (CoGM), but because of PV, it is also represented by C_1. On the other hand, central GM (CeGM), which is lighter than CoGM, is mainly represented by C_1. White matter is delineated by three labels C_1, WM and C_2.

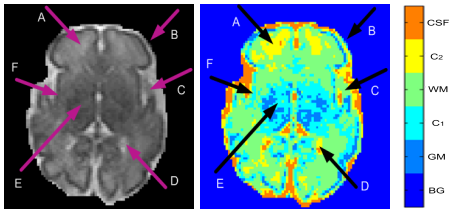

Fig. 2. T2w slice and its Bayesian classification, GM_1 and GM_2, and WM_1 and WM_2, have been respectively grouped to GM and WM. Arrows indicate PV and transition labels.

	Tissue type	Represented by label principally	Represented by label auxiliary	In fig. 2, pointed by
True	CoGM	GM	-	-
	CeGM	C_1	GM	E
	WM	WM	C_2, C_1	A
	CSF	CSF	C_2	D
PV	CSF + NB	GM	C_1	B
	CSF + GM	WM	-	C
	GM + WM	C_1	-	F
	WM + CSF	C_2	-	-

Table 1. Description of correspondence between labels and different tissues type. NB is non-brain tissue.

2.2 Spatial distribution model

After Bayesian segmentation, a MRF model allows to refine the classification of the C_1, C_2 and misclassified voxels. Note that intensity information is not considered anymore. This prevents large areas of PV to appear again. At this point, an image S is constituted of a set L of labels. By MRF theory [18], the probability for a voxel i to belong to a certain class x_i depends on its neighborhood $N = \{N_i, i \in S\}$ and on a certain energy function,

$$U_i(x) = V_i(x_i) + \sum_{j \in N_i} V_{ij}(x_i, x_j), \quad x \in L. \tag{1}$$

Labeling of x'_i of a voxel i is done by the largest energy rule

$$x'_i = \max_{\forall x \in L}(U_i(x)). \tag{2}$$

Local and global spatial information Local spatial interactions are guided by neighboring positions in the image (8-neighbors in-plane, neighbors inter-plane are not considered due to large inter slice distance). But additional spatial information must be added to reclassify large areas of PV voxels. Instead of using a probabilistic atlas as in [6, 19], here we use a cortical distance map (the CSF/CoGM transition) as represented in Figure 3. To avoid the cortical mask ($COmask$) to go too far inside brain, a limit is set beyond which CSF voxels do not increase the size of cortical mask, $CSF_{out} = \{i \mid x_i \in CSF \cap COmask(i) > 0.7\}$. Inside the brain values are computed as:

$$COmask(i) = \begin{cases} -\frac{e-k}{k} & \text{if } e \leq k \\ 0 & \text{otherwise,} \end{cases} \tag{3}$$

where k is the distance, in voxels, on which the cortical mask is effective. In our case, k was empirically set to 5. e is the distance between the voxel i and the nearest CSF_{out} voxel, $e = \min_{j \in \{CSF_{out}\}}(d(i, j))$.

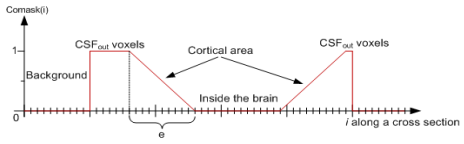

Fig. 3. Typical values of the function $COmask(i)$ along a cross section of slice

PV and misclassified voxels removal The external field $V_i(x)$ gives an entry-level weight for each voxel depending on its label. Voxel belonging to final labels

(GM, WM and CSF) receive a larger weight than transition labels:

$$V_i(x) = \begin{cases} 16 \text{ if } x \in \{GM, WM, CSF\} \\ 8 \quad \text{if } x \in \{C_1, C_2\}. \end{cases} \tag{4}$$

The MRF is done in three steps. The internal field,

$$V_{ij}(x_i, x_j) = \frac{\delta_n(x_i, x_j)}{d(x_i, x_j)}, \tag{5}$$

will change at every step, defined by δ_n energies, where n denotes the step number and d is the Euclidean distance in mm between x_i and x_j locations. First, we eliminate most PV of type non-brain/CSF by forcing every voxel with background neighbors to become CSF:

$$\delta_1(x_i, x_j) = \begin{cases} 20 \text{ if } x_j = BG \\ 0 \quad \text{otherwise.} \end{cases} \tag{6}$$

Such correction ensures also a more precise computation of the $COmask$. Second, we tackle the reclassification of C_1 voxels into either GM or WM. $COmask$ is used in this step to have different rule of energy for cortical voxels. By brain anatomy, in cortical area WM cannot be neighbor of CSF. Thus, in the cortical mask, CSF and GM label energy is increased for WM voxels neighboring CSF. This will cause CSF to expand until GM is encountered:

$$\delta_2(x_i, x_j) = \begin{cases} \beta_x(x_i, x_j) \cdot 2.5 \cdot COmask(i) & \text{, if } x \in \{GM, CSF\} \\ 0 & \text{, otherwise.} \end{cases} \tag{7}$$

β_{GM} and β_{CSF} are defined as:

$$\beta_{GM}(x_i, x_j) = \begin{cases} 2 \quad \text{if } x_i = C_1 \\ 2 \quad \text{if } x_i = WM \text{ and } x_j = GM \\ 2.5 \text{ if } x_i = WM \text{ and } x_j = CSF \\ 0 \quad \text{otherwise,} \end{cases} \tag{8}$$

$$\beta_{CSF}(x_i, x_j) = \begin{cases} 3 \quad \text{if } x_i = C_2 \text{ and } x_j = CSF \\ 1 \quad \text{if } x_i = GM \text{ and } x_j = CSF \\ 2.5 \text{ if } x_i = WM \text{ and } x_j = CSF \\ 1 \quad \text{if } x_i = WM \text{ and } x_j = GM \\ 0 \quad \text{otherwise.} \end{cases} \tag{9}$$

We assume that C_1 voxels in cortical area are PV of type GM/WM, so those voxels are reclassified as GM (Eq. 8). Eq. 9 reclassifies remaining PV of type NB/CSF (it reclassifies GM voxel surrounded by CSF). This model is stopped after no more changes are noticed (usually 10 iterations).

Last MRF energy step reclassifies C_1 into GM or WM while C_2 voxels are reclassified into WM or CSF:

$$\delta_3(x_i, x_j) = \begin{cases} 2 \text{ if } x_i = C_1 \text{ and } x_j = GM \\ 3 \text{ if } x_i = C_1 \text{ and } x_j = WM \\ 3 \text{ if } x_i = C_2 \text{ and } x_j = WM \\ 2 \text{ if } x_i = C_2 \text{ and } x_j = CSF \\ 0 \text{ otherwise.} \end{cases} \tag{10}$$

The model stops when less than 1% of voxels of transition labels change. The remaining voxels, whatever belonging to label C_1 or C_2, are reassigned as WM. At this point, only three labels remain: GM, WM and CSF. GM voxels are separated into CoGM and CeGM. To do this, a new image containing only GM and background is created. On each slice, each connected part of GM, L_{GM}, is labeled. If $\max_{i \in L_{GM}}(COmask(i)) > 0.8$, the voxel is set to $non-brain$. The rest of GM and WM voxels are set to $brain$. The largest connected $brain$ object is the final result. Figure 4 shows the result after each MRF iteration.

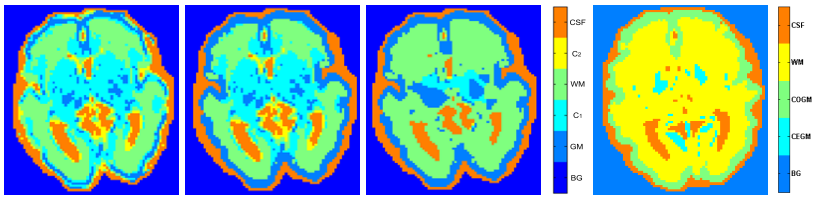

Fig. 4. Main steps of MRF: 1st, neighbors of BG are set to CSF; 2nd, CoGM; 3th, reclassification of *transition* $C's$ voxels; 4th, splitting into CoGM and CeGM.

3 Preliminary results

Manual segmentations of the CoGM and basal ganglia (BG) have been done by an expert rater. Qualitative validation is presented for one fetus only because of limited space. Similar results have been obtained for all cases. Visual comparison of CoGM contours, Fig. 5, shows that our segmentation is very similar to the manual one except close to the mid sagittal plane. Quantitative assessment is presented in Table 2. Dice Similarity Measure (DSM) is computed on the CoGM mask and Mean Euclidean Distance Error (MDE) is computed on the brain surface, see Fig. 6. BG area has not been considered in the evaluation. DSM is close to 0.7 (above whom is considered a good overlap) but not reaching such value. This is because manual and automated segmentation often differ in the GM/WM interface. On the contrary, qualitative and quantitative evaluation regarding the brain surface (CSF/GM interface) shows a much better agreement. Distance errors in brain surface are very low as seen in Fig. 6.

Name (GA)	Case 19 (30)	Case 23 (29)	Case 22 (32)	Case 20 (31)
DSM on CoGM mask	0.64	0.68	0.58	0.60
Manual CoGM volume (total number of voxels)	8060	7405	12480	10158
Automated CoGM volume (total number of voxels)	10108	9995	8775	7520
MDE (per pixel in mm)	0.7874	0.7644	0.6126	0.6253

Table 2. Quantitative evaluation compared to manual segmentation.

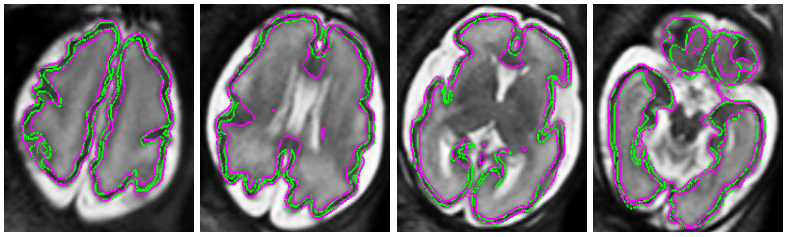

Fig. 5. Manual segmentation (green) and automated segmentation (pink).

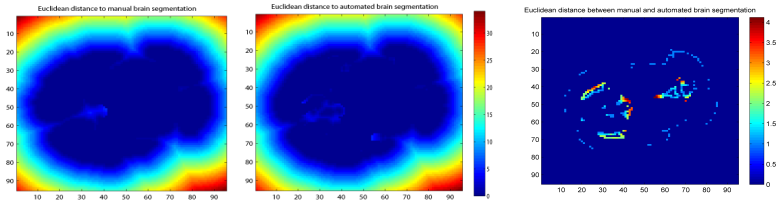

Fig. 6. Euclidean distance to brain surface: manual and automated. Squared error.

4 Discussion

We have presented a new image and spatial distribution model for automated segmentation of MR fetal images. Validation is challenging since no gold standard is available, however comparison to an expert segmentation has been shown. Our results are preliminary and we are currently processing more subjects that we will include in future work. Current main limitations are the precision in deep sulci and the errors performed at central nuclei structures, so that we needed to exclude basal ganglia from the segmentation process. Future work may include automatic segmentation of the subcortical gray matter. This work is only the first step for a quantitative fetal brain development analysis method. Indeed, we are working on reconstruction of high resolution fetal brain, combining the 6 acquired axial volumes, with compensation for intra-volume and inter-volume motion in the images as introduced in [14]. Future work include the combination of the brain segmentation as presented here in a high resolution space.

References

1. M. Rutherford et al.: MR imaging methods for assessing fetal brain development. Developmental Neurobiology **68**(6) (2008) 700–711
2. L. Guibaud: Contribution of fetal cerebral MRI for diagnosis of structural anomalies. Prenatal Diagnosis **29**(4) (2009) 420–33
3. H. Xue et al.: Automatic segmentation and reconstruction of the cortex from neonatal MRI. NeuroImage **38**(3) (2007) 461–477
4. J. Dubois et al.: Mapping the early cortical folding process in the preterm newborn brain. Cerebral Cortex **18** (2008) 1444–1454

5. H. Merisaari et al.: Quantitation of the premature infant brain volume from MR images using watershed transform and bayesian segmentation. In: 15th European Signal Processing Conference. (2007)
6. M. Prastawa et al.: Automatic segmentation of mr images of the developing newborn brain. Medical Image Analysis **9** (2005) 457–466
7. I. Claude et al.: Fetal brain MRI: Segmentation and biometric analysis of the posterior fossa. IEEE Trans. on Bio. Eng. **51**(4) (2004) 617–626
8. P.A. Habas et al.: Atlas-based segmentation of the germinal matrix from in utero clinical mri of the fetal brain. Med Image Comput Comput Assist Interv Int Conf Med Image Comput Comput Assist Interv **11**(Pt 1) (2008) 351–8
9. N. Weisenfeld et al.: Segmentation of newborn brain MRI. In: IEEE Intl Symp on Biomedical Imaging. (2006)
10. P. Huppi et al.: Quantitative magnetic resonance imaging of brain development in premature and mature newborns. Annals of Neurology **43** (1998) 224–235
11. A. Zacharia et al.: Early assessment of brain maturation by MR imaging segmentation in neonates and premature infants. AJ of Neuroradiology **27** (2006)
12. P. Anbeek et al.: Probabilistic brain tissue segmentation in neonatal magnetic resonance imaging. Pediatric Rechearch **63**(2) (2008) 158–163
13. Z. Song et al.: Clinical neonatal brain MRI segmentation using adaptive nonparametric data models and intensity-based Markov priors. MICCAI (2007) 883–890
14. D. Ferrario et al.: Brain surface segmentation of MRI of the fetus. In: 16th European Signal Processing Conference. (2008)
15. www.itk.org: Insight registration and segmentation toolkit
16. M. Styner, et al.: Parametric estimate of intensity inhomogeneities applied to MRI. IEEE Trans. on Medical Imaging **19**(3) (2000) 153–165
17. K. Van Leemput, F. Maes, D. Vandermeulen and P. Suetens: Automated model-based bias field correction of mr images of the brain. IEEE Transactions on Medical Imaging **18** (1999) 885–896
18. Besag, J.: Spatial interaction and the statistical analysis of lattice systems. J. Roy. Statist. Soc. **36** (1974) 192–326
19. N. Weisenfeld et al.: Highly accurate segmentation of brain tissue and subcortical gray matter from newborn MRI. In: MICCAI. (2006)